

# MediViSTA-SAM: Zero-shot Medical Video Analysis with Spatio-temporal SAM Adaptation

Sekeun Kim<sup>a</sup>, Kyungsang Kim<sup>a</sup>, Jiang Hu<sup>a</sup>, Cheng Chen<sup>a</sup>, Zhiliang Lyu<sup>a</sup>, Ren Hui<sup>a</sup>, Sunghwan Kim<sup>a,c</sup>, Zhengliang Liu<sup>d</sup>, Aoxiao Zhong<sup>b</sup>, Xiang Li<sup>a</sup>, Tianming Liu<sup>d</sup>, Quanzheng Li<sup>a</sup>

<sup>a</sup>Center of Advanced Medical Computing and Analysis, Massachusetts General Hospital and Harvard Medical School, Boston, MA 02114, USA

<sup>b</sup>Harvard John A. Paulson School of Engineering and Applied Sciences, Harvard University, Cambridge, MA 02138, USA

<sup>c</sup>Department of Thoracic and Cardiovascular Surgery, Gyeongsang National University Changwon Hospital, Gyeongsang National University College of Medicine, Changwon, Republic of Korea

<sup>d</sup>School of Computing, The University of Georgia, Athens, GA 30602, USA

## Abstract

The Segmentation Anything Model (SAM) has gained significant attention for its robust generalization capabilities across diverse downstream tasks. However, the performance of SAM is noticeably diminished in medical images due to the substantial disparity between natural and medical image domain. In this paper, we present a zero-shot generalization model specifically designed for echocardiography analysis, called MediViSTA-SAM. Our key components include (i) the introduction of frame-level self-attention, which leverages cross-frame attention across each frame and its neighboring frames to guarantee consistent segmentation outcomes, and (ii) we utilize CNN backbone for feature embedding for the subsequent Transformer for efficient fine-tuning while keeping most of the SAM's parameter reusable. Experiments were conducted using zero-shot segmentation on multi-vendor in-house echocardiography datasets, indicating evaluation without prior exposure to the in-house dataset during training. MediViSTA-SAM effectively overcomes SAM's limitations and can be deployed across various hospital settings without the necessity of re-training models on their respective datasets. Our code is open sourced at: <https://github.com/kimsekeun/MediViSTA-SAM>

## 1. Introduction

The field of artificial intelligence (AI) has undergone a significant transformation, driven by the emergence of large-scale models such as the large language model GPT Brown et al. (2020) and the text-to-video generative AI model SORA openai (2024). These models, trained on extensive datasets and utilizing abundant computational resources, have enabled significant achievements across various tasks. Segmentation Anything Model (SAM) Kirillov et al. (2023) is a vision foundation model designed for promptable image segmentation, trained on annotated dataset (SA-1B) on 11 million natural images. Due to pretrained on large dataset, SAM has demonstrated impressive zero-shot performance on various tasks in the context of natural images. The success of SAM has attracted interest in their potential applications in more specialized fields. While SAM demonstrates impressive performance with natural images, its effectiveness noticeably diminishes when applied to medical images, mainly due to the significant disparity between the domains of natural and medical image Wald et al. (2023).

A recent consensus among researchers suggests that research should focus on development of medical foundation model using large dataset to generalize across various demographics, types of imaging equipment, and protocols Zhou et al. (2023); Chen et al. (2024). The development of a new foundational model for medical images is feasible; however, the primary challenge lies in the significantly lower availability of medical images and high-quality annotations compared to natural images. Obtaining qualified data for training medical AI models demands expertise from domain specialists, resulting in considerable costs and time investments. Particularly, unlike CT or MRI, which have abundant public datasets, other modalities like echocardiography lack large sets of public data. In model perspective, the Vision Transformer (ViT) typically requires extensive datasets for effective training Dosovitskiy et al. (2020) to achieve superior properties in general medical image analysis. To address these challenges, recent studies have increasingly focused on

adapting SAM for medical image analysis. The use of pretrained models as initialization is renowned for enhancing performance and converge speed in medical image analysis tasks Kalapos and Gyires-Tóth (2022) by lowering computational demands. Two main approaches have emerged. The first involves prompt engineering Deng et al. (2023), which aims to generate precise instructions such as points, bounding boxes, and masks to accurately segment each object within the image. However, the selection of optimal prompts necessitates prior knowledge. For instance, in medical image analysis, detection networks are indispensable for choosing point prompts. Second approaches, employ parameter-efficient transfer learning (PETL) techniques, such as LoRA Hu et al. (2021) or Adapters Wu et al. (2023), demonstrate promising performance in segmentation integrated without modifying the core architecture and designed to fine-tune the model's response to the specific challenges presented by medical imaging. This approach leverages existing knowledge derived from natural images, integrating it with detailed, task-oriented insights specific to the medical field.

Although 2D images are common in natural image, medical imaging often extends into the third dimension to capture volumetric details. Imaging modalities such as CT and MRI scans provide volumetric insights that are essential for comprehending anatomical structures and pathologies. However, the 2D-focused design of SAM does not support these images. Adapting SAM to accommodate 3D data would likely require modifications to its architecture, possibly including the integration of 3D convolutional layers or volumetric transformers. Many efforts have been proposed to extend 2D medical image analysis to 3D volumetric images Bui et al. (2023); Chen et al. (2023). However, the true potential of a foundational model lies in its ability to generalize across modalities that suffer from a scarcity of datasets, such as echocardiography, a widely utilized and cost-effective imaging technique in clinical settings. The real power of foundation model lies in application in modalities with lack of dataset, such as echocardiography, which is most frequently used in clinical practice with low cost. However, there has been comparatively less researches on medical video analysis even it is crucial for clinical practice. Analyzing medical video data necessitates a

\*This is an example for title footnote coding.

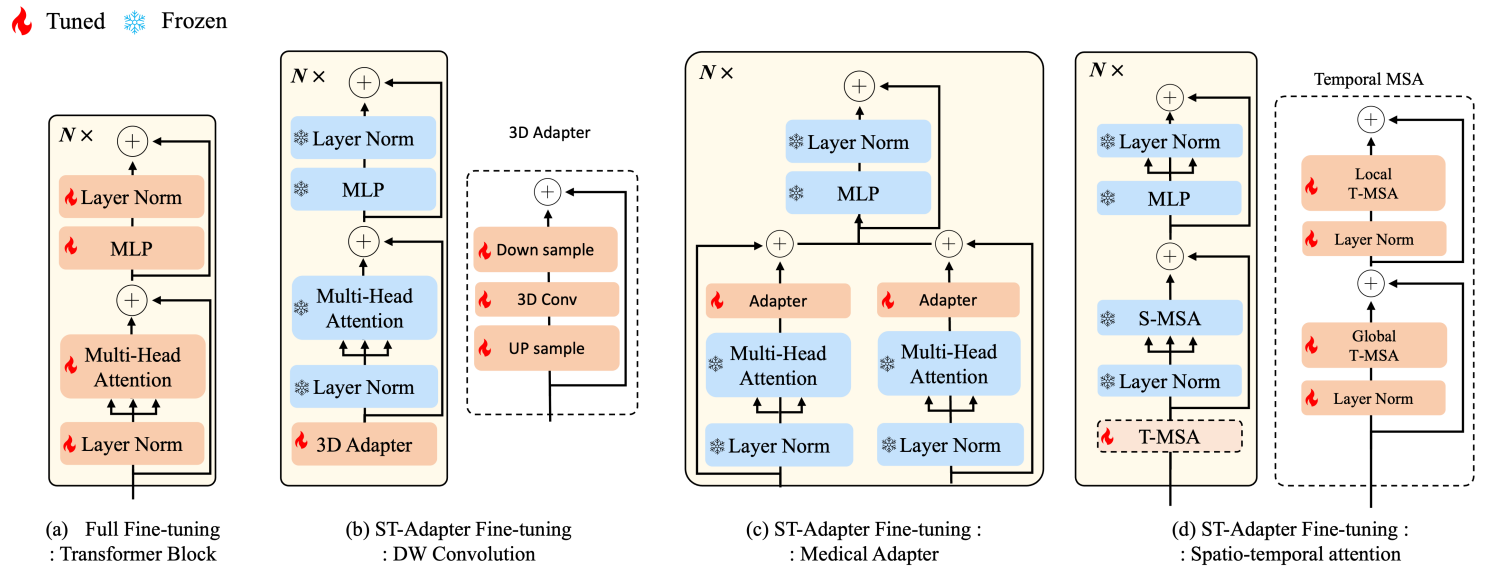


Figure 1: Image-to-video transfer learning strategies. (a) Vanilla transformer block (b) 3D adapter with depthwise 3D convolution (Pan et al., 2022) (c) 2D image to 3D adapter (Wu et al., 2023) (d) Proposed medical video spatio-temporal adapter (MediViSTA).

deep understanding of both the spatial information, which includes the varying sizes of objects, and the temporal dynamics essential for precise object boundary delineation. This task is further complicated by the presence of artifacts in ultrasound image, where ambiguous boundaries may not be clearly discernible in certain frames, yet become more clear in subsequent ones.

While SAM have seen success in CT and MRI modalities due to the abundance of annotated public datasets, the situation become worse in echocardiography which have sparse dataset only have annotation for the end-diastole and end-systole phase. As a result, the difficulties in tuning large network SAM’s basic transformer blocks may not optimal for echocardiography. Although to overcome the limitation of convolution neural network (CNN) in learning global relationships between pixels, the Vision Transformer (ViT) was introduced to model global dependency between pixels through self-attention mechanisms. The limitation of transformer that requires the large number of training dataset to learn global dependency among pixels through the self-attention mechanism. The choice of an appropriate approach is therefore critical for effective network design.

In this paper, we propose a efficient architecture with parameter-efficient adaptation method to adapt SAM from 2D to the medical video 2DT segmentation task especially for echocardiography. Distinct from previous SAM based adaptation method, we embedded 2DT input with a simple CNN encoder. We freeze the SAM’s encoder and leverage it as the feature extractor to utilize SAM’s generalizable knowledge learned from large dataset. To learn temporal relation efficiently between each frames, we divided the 2DT input along the time dimension, and then the temporal adapter to generate the feature maps. We propose a temporal adapter consist of global and local temporal attention blocks. This strategy proves to behave well to overcome the limitation the discontinuity issue caused by frame by frame segmentation, and also improve overall segmentation results. Lastly, we utilize lightweight mask decoder deisgn with multi-scale fusion to deal with varying object and ROI scale in echo scan. We conduct experiments on echocardiography segmentation datasets with comprehensive comparisons with domain SOTA approaches, as well as adapters in general. The results show our methods can outperform existing methods by a large margin, and notably our method shows significantly high performance on zero-

shot analysis in-hospital dataset from Massachusetts General Hospital (MGH) and Brigham and Women Hospital. Our contributions are summarized as follows:

- We present the Adaptation approach for echocardiography video segmentation. Our framework, is a simple yet effective extension of SAM architecture, significantly improving capabilities in echocardiography analysis.
- We proposed MediViSTA-SAM, designed to facilitate the segmentation of high-dimensional medical video data by adapting the SAM architecture for enhanced ability. Specifically, MediViSTA-SAM is engineered to capture both global and local temporal information through a cross-frame attention mechanism, capturing dependencies between frames effectively. This method extend the capabilities of the 2D SAM model, significantly enhancing its performance in echocardiography segmentation.
- We conduct comprehensive experiments of our methods using zero-shot analysis in-house data collected from various centers and vendors. The results demonstrate the exceptional ability of our models to generalize performance on in-house dataset.

## 2. Related Work

### 2.1. Large-scale Vision Foundation Models

The large-scale model, key contributors such SegGPT Wang et al. (2023), SEEM Zou et al. (2023), CLIP Radford et al. (2021), have made significant contributions in foundation model. Their remarkable zero-shot and few-shot generalization capabilities enable prompt adaptation and extension to specified tasks or domains, predominantly through pre-training and subsequent fine-tuning methodologies. Also, change enabling rapid adaptation and extension to target tasks or domains through pre-training and fine-tuning paradigms. SegGPT unifies segmentation and contextual learning using through transforming diverse segmentation data into images of a standardized format. This allows for a more comprehensive understanding of the image content. SEEM Zou et al. (2023) proposes a interface that utilizing the various sources to effectually segment and categorize contents in images or videos concurrently. CLIP Radford et al. (2021) proposes a unified

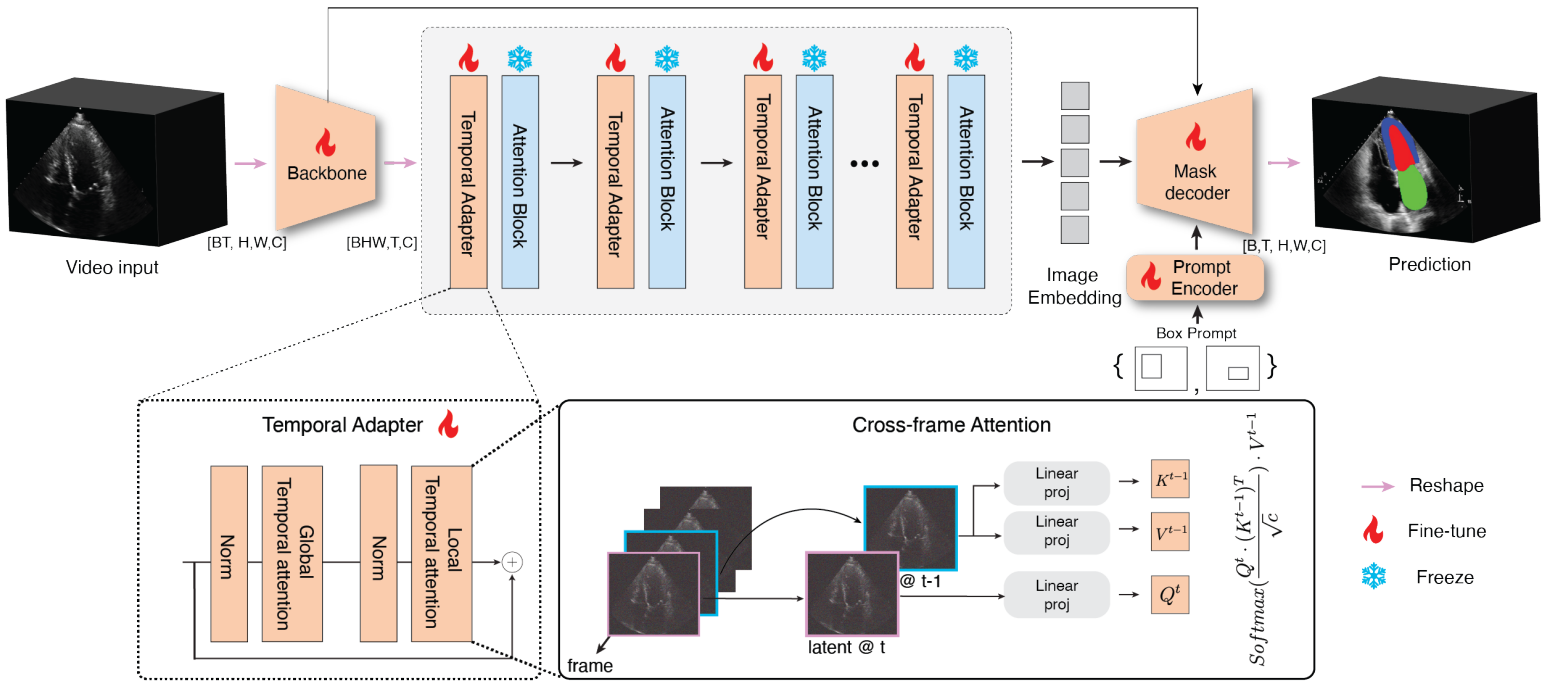


Figure 2: Structure comparison of different SAM-based foundation models for medical 3D or 2DT analysis. (a) Vanilla transformer block (b) 3D adapter with depth-wise 3D convolution Pan et al. (2022) (c) 2D image to 3D adapter Wu et al. (2023) (d) Proposed spatio-temporal adapter for medical video analysis (MediViSTA-SAM).

vision and language model that can be utilized for various downstream tasks, such as classification, and visual questioning task. SAM Kirillov et al. (2023), distinguished for its zero-shot and few-shot capabilities, has been acknowledged for its effectiveness in specific tasks or domains, attributed to its adaptability and broad applicability.

## 2.2. Parameter-efficient fine-tuning

The emergence of large-scale foundational models has made Parameter-Efficient Fine-Tuning (PEFT) increasingly popularity. It recognized as an effective method for adjusting a large-scale model to specific application. Unlike full fine-tuning, PEFT maintains the majority of parameters unchanged and adjusts a much smaller fraction. This approach facilitates quicker updates and more efficient learning processes without catastrophic forgetting and generalize better to out-of-domain adaptation Zaken et al. (2021). PEFT technique can be categorized into three main types: addition-based approaches Pan et al. (2022), which integrate lightweight adapters or prompts Jia et al. (2022) into the base model, affecting only these added elements; specification-based techniques Zaken et al. (2021), which fine-tune a select few of the original parameters; and reparameterization strategies Hu et al. (2021), employing low-rank matrices to updates minimum number of trainable parameter.

To extend 2D designed model into the third dimension to capture volumetric or temporal details, several adapters are shown in Figure 1. ST-Adapter Pan et al. (2022) incorporates 3D convolution layer in each transformer block to capture spatial-temporal features for recognition tasks as in Fig 1 (b). However, it increases computational cost with increasing video clips and degrade training efficiency. To make the 3D adapters compatible with the 2D SAM backbone, a reshape operation is applied to transform by merging the adjacent slices into batch dimension in Fig.1 (c). Understanding the temporal dimension of data is crucial for medical video analysis. Time sequence modeling can be broadly categorized into two approaches. The first approach focuses on leveraging extracted features from individual frames or directly processing videos seamlessly to model temporal data. Typically, this involves extracting motion features between frames,

such as optical flow, to capture temporal information. The second approach involves extracting features while considering the temporal aspect of data as depth information using 3D convolutions Qiu et al. (2017) This approach offers a more adaptable prompting system for open-set segmentation tasks. Once features are extracted from video frames, standard sequence models like LSTMs Pfeuffer et al. (2019) or Transformers can be applied to handle various tasks. These models aim to capture dependencies within sequences, either through recurrent neural networks or self-attention mechanisms. For modeling long sequences and time series, is gaining attention in sequence modeling. For end-to-end video modeling, transformer adaptations such as Video Swin Transformer Hatamizadeh et al. (2021), and TimeSformer Bertasius et al. (2021) are popular choices. We utilized 2D SAM’s backbone and apply temporal adapter consist global temporal and local temporal attention as in Figure 1 (c).

## 3. Methodology

### 3.1. Segment anything model

We provide an initial overview of the Segment Anything Model (SAM). SAM consist of three core components: an image encoder, a prompt encoder, and a mask decoder. The image encoder utilizes a standard Vision Transformer (ViT) architecture, which has been pre-trained through a Masked Autoencoder (MAE) approach in an unsupervised manner. The author has officially released three pretrained models, which are ViT-B/16, ViT-L/16, and ViT-H/16, corresponding to base, large and huge model and patch size. The embedded output feature of image encoder is downsampled by a factor of 16 from the input image. The prompt encoder can be categorized as either using sparse point points and boxes or dense mask prompts. The mask decoder features a modified Transformer decoder block, equipped with a dynamic mask prediction head. This decoder’s cross-attention mechanisms to learn the interaction between prompt and image embeddings. Following this, SAM enhances the resolution of the image embedding, and a Multilayer Perceptron (MLP) transforms the output token into inputs

for a dynamic linear classifier. This classifier is then used for predicting the target mask of the given image.

### 3.2. Adapting SAM for video inputs

#### 3.2.1. Overall Architecture

The original SAM was designed within a 2D framework; however, medical data often comprises 2DT or 3D formats, incorporating third-dimension information. The third-dimension information is important for accurately capturing the movement of organs, like the heart, providing a more detailed and comprehensive analysis. Our goal is to enhance the capability of the SAM model for analyzing medical videos, adapting it from its original architecture designed for 2D natural images. To maximize SAM’s generalization ability with large training dataset, we utilize the pretrained SAM parameter in a frozen, rather than update all parameters. This approach allows us to utilize the strength of the SAM model while efficiently adapting it for the complexities of medical video data.

#### 3.2.2. Encoder design

As a backbone encoder to extract high-level feature, we used feature map in last layer of CNN backbone used in the subsequent transformer, and feature maps in each layer of CNN backbone to mask decoder Chen et al. (2021); Park et al. (2022). This architecture embeds multi-scale feature representations for each layer, combining these high-level feature representations to achieve segmentation results with the Transformer is one of the fundamental concepts of our approach. More detailed experimental results about the role of CNN encoder will be provided within ablation studies of Table 3.

Current approaches for adapting 2D pretrained models to 3D or 2DT applications typically handle images on a slice-by-slice basis, employing spatial adaptors to integrate the 2D data. Because the backbone consists of transformer blocks designed for 2D input, to this end, we consider our adapter especially for echocardiography which have limited motion between frames. Previous studies in video generation tasks have shown the effectiveness of cross-frame attention techniques in learning temporal dependencies and incorporating contextual information across video frames Khachatrian et al. (2023) introduced the concept of cross-frame attention to anchor the object’s appearance and shape in the initial frame of video, which in effectively generate subsequent video frames.

However, relying solely on anchoring the first frame with cross-frame attention is inadequate when dealing with intermittent noise and image obscuration, especially in medical images such as echocardiography Mitchell et al. (2019). To address this issue, we redesigned cross-frame attention mechanism that capitalizes on the approach of using the immediately preceding video frame as a constraint. More specifically, self-attention layer receives the latent feature  $v_i \in \mathbb{R}^{(B \times H \times W) \times T \times C}$  of  $I_i$ , and linearly projects  $v_i$  into query, key, and value ( $Q, K, V$ ) to produce the output of self-attention as follows:

$$Q = W^Q v_i, \quad K = W^K v_i, \quad V = W^V v_i \quad (1)$$

The self-attention output is calculated using the following equation:

$$\text{Self\_Attn}(Q, K, V) = \text{Softmax}\left(\frac{Q^t \cdot (K^{t-\delta})^T}{\sqrt{d}}\right) V^{t-\delta} \quad (2)$$

where  $t$  indicates frame,  $\delta$  is step size. On the contrary, the cross-frame attention employs the key and value from the first frame, along with the query from the current frame. We integrate information from both the current frame and the frame occurring at a time step  $\delta$  preceding the current frame. The specific value of  $\delta$  can be determined according to the frame rate of the scanned image.

The overall architecture of our proposed model is provided in Figure 2. For a given video input  $X \in \mathbb{R}^{B \times C \times T \times H \times W}$ , where  $B$  indicates batch size,  $H \times W$  represents embedding dimension,  $T$  indicates total number of frames, and  $C$  denotes the input channels. In backbone, we applied reshape operation to transform video input into  $X \in \mathbb{R}^{(B \times T) \times C \times H \times W}$  to pass into the CNN encoder. In transformer blocks, we modified the transformer block incorporates spatio-temporal attention, especially temporal attention composed of global and local temporal attention to efficiently process information along the third dimension. To make the temporal attention compatible with the 2D SAM backbone, the reshaped embedded feature shape of  $(B \times H \times W) \times T \times C$  passed into the global temporal attention since it spans the temporal axis. Following global temporal attention, we apply local temporal attention, called cross-frame attention, referred to as cross-frame attention, to identify and establish dependencies between adjacent frames. Then, reshaped feature shape of  $(B \times T) \times H \times W \times C$ , we pass features into pretrained SAM’s transformer which is spatial attention since it operates within the spatial axis.

#### 3.2.3. Decoder design

As discussed in the preceding section, to leverage the advantages of both CNN and the pretrained SAM, we have devised an image encoder and made modifications to SAM’s lightweight mask decoder. In the image encoder, we employ a CNN-based encoder to extract features while progressively downsampling input image. Within the modified SAM’s mask decoder, consisting of two layers of transpose convolution, we employed four CNN decoder layers to interact with multi-scale encoder features while keeping the prompt encoder architecture. This effectively combine the strengths of both CNN and self-attention mechanisms, thereby enhancing the model’s performance in feature extraction and segmentation tasks. Our experimental evaluations have demonstrated the improved performance of our model, as illustrated in Table 4, confirming the effectiveness of our multi-scale fusion strategy.

## 4. Experiment settings

### 4.1. Datasets and implementation details

In this study, we employed the publicly available CAMUS to train all the models presented. On the other hand, the multi-center in-house dataset was exclusively used as the testing set in our study.

#### 4.1.1. CAMUS Dataset

CAMUS contains 1,000 patients’s two-dimensional (2D) echocardiography, comprising both apical two-chamber (2CH) and four-chamber (4CH) views of 500 patients. It provides sparse annotation along the cardiac cycle only at end-diastole (ED) and end-systole (ES). The ground truth of three structures the left ventricle  $LV_{endo}$ , the epicardium  $LV_{epi}$ , and the left atrium (LA) for 2CH and 4CH are provided. Half of the patients have an ejection fraction(EF) lower than 45%, 19% of the images have poor quality.

Concerning the aspect of variability, the CAMUS dataset reveals a substantial spectrum of dice similarity coefficients (Dice) in relation to both inter and intra variability, as assessed by experienced experts. In the case of the CAMUS dataset, we utilized 402 patients for training the model, while the remaining 98 patients were reserved for testing. Specifically, the testing dataset comprised full-cycle apical 4-chamber (A4C) sequences, and it included dense annotation data for  $LV_{endo}$  and  $LV_{epi}$ , as made available by Painchaud et al. (2022).

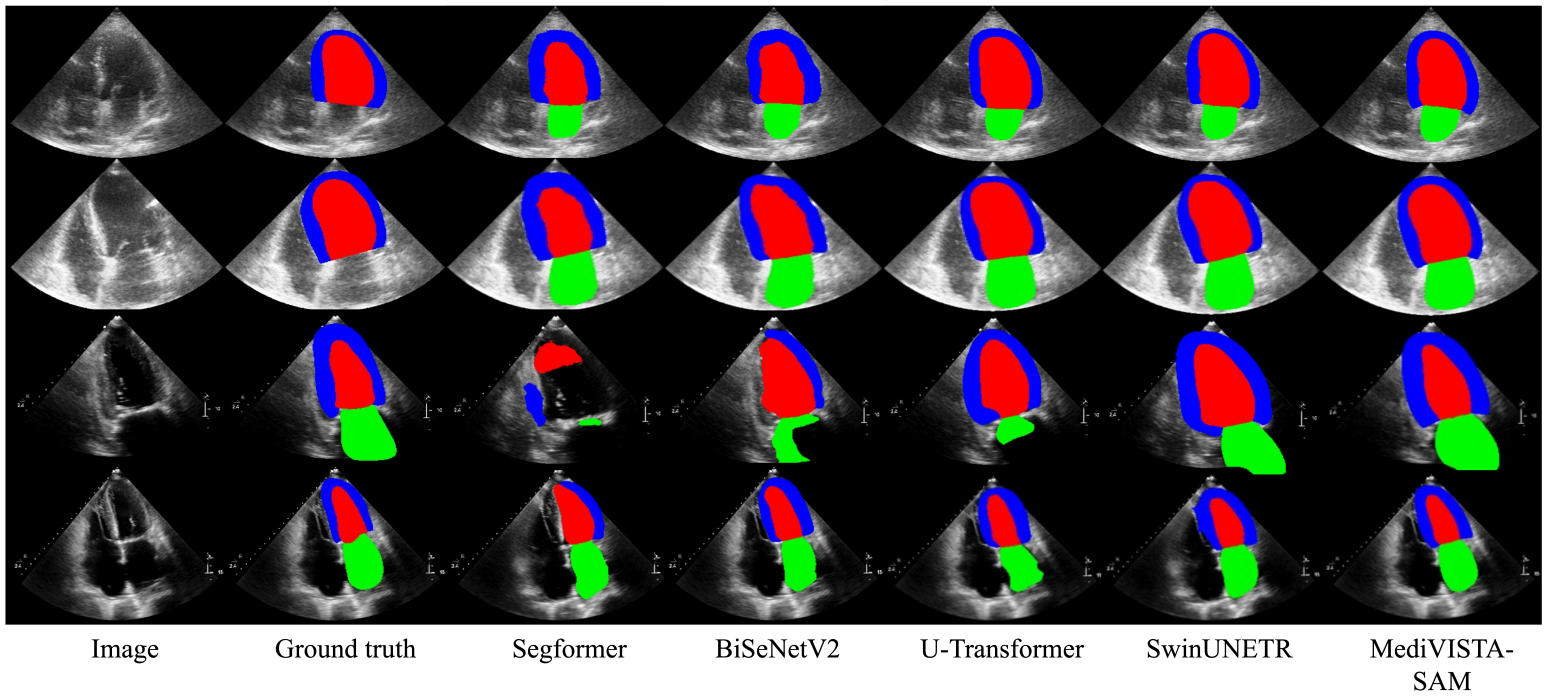


Figure 3: The visual comparison of segmentation results on CAMUS dataet (rows 1-2) and our in-house dataset (rows 3-4). The blue, red and green regions denote the left ventricle epicardium, endocardium and left atrium, respectively. Please note that the CAMUS sequential dataset only includes labels for  $LV_{endo}$  and  $LV_{epi}$ .

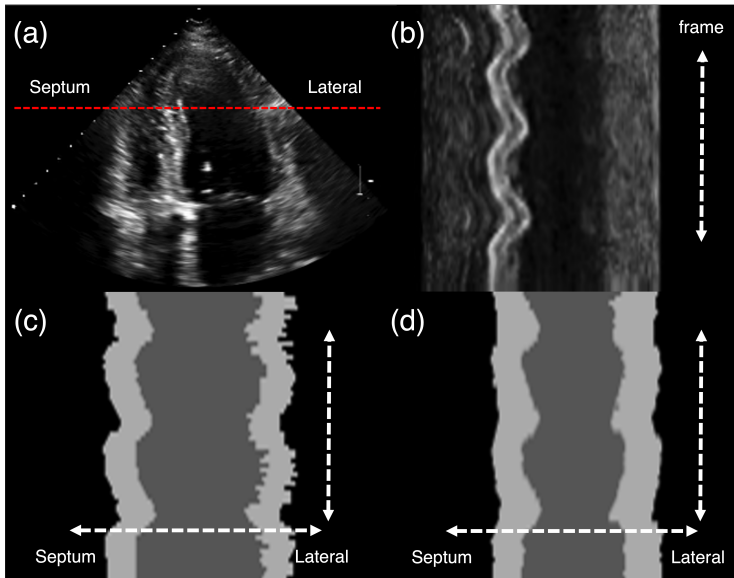


Figure 4: The effect of cross-frame attention on a patient with a heart rate exceeding 100 beats per minute (bpm). (a) B-mode image (b) radial image cut spanning the entire time sequence (c),(d) segmentations without and with cross-frame attention, respectively.

#### 4.1.2. In-house Dataset

We collected an multi-center dataset consists of B-mode echocardiography images from 100 patients consists of apical two and four-chamber view (A2/4C). It was collected from two hospitals with two different imaging vendors, including GE and Philips, utilizing their respective flagship models, the Vivid E95 and the Philips EPIQ 7C. Each manufacturer contributed equally, providing samples from 50 patients each, thereby ensuring a balanced representation in the study. The images were collected at the Massachusetts General Hospital and Brigham and Women’s Hospital between 2017 and 2022 who needs a clinical care.

The annotation process was undertaken with utmost precision by two skilled clinicians. The annotation include the boundaries of the Left Ventricle endo ( $LV_{endo}$ ), Left ventricle epicardium ( $LV_{epi}$ ), and Left Atrium (LA) during the end-diastole (ED) and end-systole (ES) phases. Given the intermittent noise and image obscuration in images, the clinicians meticulously examined adjacent frames in the video sequences to pinpoint and define accurate boundaries. following the recommendations of the American Society of Echocardiography Lang et al. (2015). This annotation process was accomplished using the Slicer 3D software Fedorov et al. (2012), a tool well-regarded for its precision in medical imaging analysis.

#### 4.1.3. Implementation details

Our model was trained using the Dice loss function with an ignore index. In this context, the ignore index represents frames in the dataset that do not have any annotations. Frames that do have annotations are assigned labels, while those without annotations are designated with the ignore index. This approach helps us manage the problem of label imbalance during training by effectively ignoring frames that lack annotations. A MADGRAD optimizer Defazio and Jelassi (2022) with a learning rate of  $10^{-4}$  is used for training. We employed gradient norm clipping to avoid exploding gradients and a soft constraint for the vanishing gradients problem and ensuring effective convergence, a gradient norm clipping was applied with a maximum norm of 1.0. In the pre-processing, we selected one cardiac cycle comprising 32 frames to more effectively address the SAM issue. The image intensities, initially ranging from  $[0, 255]$ , were normalized to a scale between  $[0, 1]$  using min-max normalization technique. To maintain a consistent input size that includes one complete cardiac cycle, we sampled images during the period between end-diastole (ED) and end-systole (ES) phases. In cases where the desired number of frames was not obtained through this method, we conducted additional sampling after the ES frame to ensure that the required number of frames was acquired. We constructed our proposed model on the Pytorch platform, leveraging the computing power of 8 NVIDIA A100 GPUs.

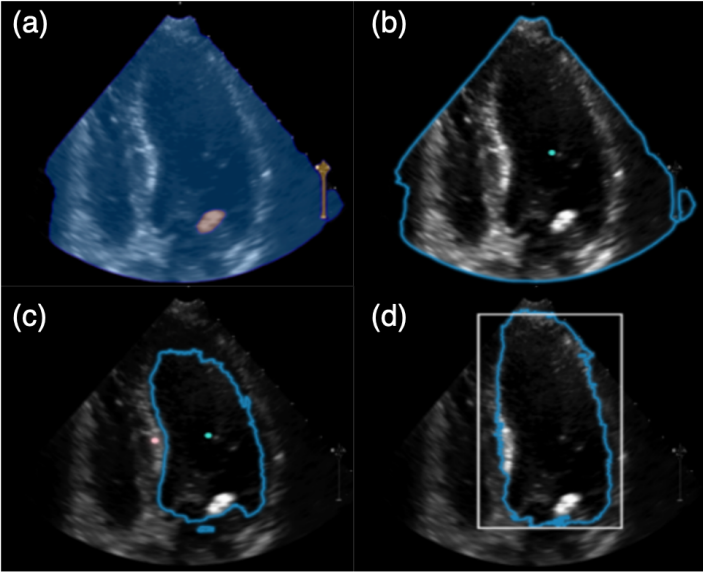


Figure 5: Results of qualitative comparisons across various prompts. (a) no prompt (b) one point prompt (c) two points prompts (d) bounding box prompts, respectively. The green dot indicates the point to be included as prompts, while the red dot represents the point to be excluded. The segmentation results with blue are overlaid on input image.

## 4.2. Evaluation Metric

### 4.2.1. Region based metrics

In our study, we use three region based metrics to assess segmentation precision, including the Dice coefficient, Hausdorff distance, and Average Symmetric Surface Distance (ASSD). The Dice coefficient is a statistical tool that quantifies the overlap between the actual and predicted segmentation areas. The Hausdorff distance measures the greatest distance from a point in one set to the closest point in the other set. Additionally, we employ the Average Surface Distance (ASD) metric to determine the mean distance between binary objects found in two segmented images, providing a comprehensive view of segmentation accuracy and consistency.

### 4.2.2. Temporal Consistency Indicator

To evaluate the temporal smoothness in the segmentation results, we normalize each video with varying total frames to a range of 0 to 1. For assessing temporal smoothness, we analyze how smooth the segmentation pixels  $s_a$  transition across frames. We analyze its second-order derivative. A high derivative value suggests periods of substantial variation, while a lower derivative indicates local smoothness. Given the discrete nature of cardiac time frames, we approximate the second-order derivative numerically as described in Painchaud et al. (2022):

$$\frac{d^2 s_a(t)}{dt^2} \approx s_{a,t+1} + s_{a,t-1} - 2s_{a,t} \quad (3)$$

This approximation functions act as a Laplacian filter, evaluating the temporal alignment of three consecutive values across the cardiac cycle. We then measure the difference between each data point and the average of its neighboring data points, providing us with a measurable indicator of temporal consistency,  $L$ . This metric demonstrates that a large derivative means significant fluctuation, whereas a small derivative indicates a localized smoothness.

### 4.2.3. Clinical metrics

The Left Ventricular Ejection Fraction (LVEF) is a critical measure that indicates the percentage of blood ejected from the heart’s main pumping chamber, commonly used to evaluate cardiac function and performance. Following the clinical guidelines for echocardiography Lang et al. (2015), we evaluate our method using the biplane simpson’s method, a common approach for estimating the volume of the left ventricle (LV) of the heart. After segmenting the left ventricle (LV) from both the 2-chamber and 4-chamber views, the ventricle is then divided into multiple disks or slices using contour information, with the volume of each disk or slice calculated individually.

$$V = \frac{\pi}{4} \sum_1^n D_i^2 \times \frac{L}{n} \quad (4)$$

where  $V$  is the volume of the left ventricle  $L$  is the length of the long axis.  $D$  is the diameter of the disk.  $n$  is number of disks, typically with a value of 20. The total volume of the ventricle is then calculated by summing the volumes of all the disks. The ejection fraction (EF) can be calculated as follows:

$$EF = \left( \frac{EDV - ESV}{EDV} \right) \times 100\% \quad (5)$$

where  $EF$  is the ejection fraction,  $EDV$  is the end-diastolic volume, and  $ESV$  is the end-systolic volume, respectively.

## 5. Results and Analysis

### 5.1. Comparison with State-of-the-Art Methods

We have conducted an extensive evaluation of our methods in two datasets: CAMUS and in-house multi-center dataset. We evaluated the performance against state-of-the-art (SOTA) methods including six CNN-based methods : LUNet Leclerc et al. (2020), Deeplabv3 Chen et al. (2017), Unet++Zhou et al. (2019), EnetPaszke et al. (2016), IC-Net Zhao et al. (2018), and BiSeNetV2 Yu et al. (2021) and three transformer based methods: SegFormer Xie et al. (2021), U-transformer Petit et al. (2021), and SwinUNETR Hatamizadeh et al. (2021). Table 1 presents outcomes for both the CAMUS and in-house datasets. The CAMUS dataset contains two labels:  $LV_{endo}$  and  $LV_{epi}$ . In contrast, the in-house dataset includes an additional label, LA, thereby covering three labels.

Across all methods, the segmentation performance for  $LV_{endo}$  and  $LV_{epi}$  in the CAMUS dataset was relatively comparable. However, as highlighted in Table 1, our approach surpassed the leading method by achieving a Dice score improvement of 1.9% and 0.2%, respectively, and by enhancing the temporal smoothness by 0.03. SAM with one point prompt have failed to generate plausible results as in Figure 5 which only segment the scan of region. Furthermore, when it comes to segmenting for the  $LV_{epi}$ , which surrounds the  $LV_{endo}$ , none of the prompt methods achieve successful segmentation. Therefore, we only include the results using two points prompts and box prompts as in Table 1. We compared MediViSTA-SAM with and without the box prompt; however, we observed no significant difference between the two outcomes. Given that using the box prompt requires human intervention, we opted not to employ box prompts in all experiments. We presented the results without applying any post-processing to facilitate a direct comparison of the segmentation capabilities across models.

### 5.2. Evaluation of Zero-shot Generalization

Evaluating the generalization capability of a model is of paramount significance. This is especially important in the medical field where

Table 1: Comparison of MediViSTA-SAM with SOTA segmentation methods on CAMUS data. Best results are denoted as **bold**. The grey background denotes the methods are proposed. Four metrics are assessed: the Dice coefficient, Hausdorff distance, Average Symmetric Surface Distance, and Laplacian temporal alignment, respectively.

CAMUS data	$LV_{endo}$				$LV_{epi}$			
	Dice $\uparrow$	dH(mm) $\downarrow$	dA(mm) $\downarrow$	$L\downarrow$	Dice $\uparrow$	dH(mm) $\downarrow$	dA(mm) $\downarrow$	$L\downarrow$
LUNet (Leclerc et al., 2020)	91.3	7.66	1.73	0.08	80.0	11.10	1.84	0.22
Deeplabv3 (Chen et al., 2017)	92.6	6.23	1.19	0.07	84.1	8.42	1.21	0.14
Unet++ (Zhou et al., 2019)	93.1	6.42	1.20	0.08	83.4	9.44	1.42	0.12
Enet (Paszke et al., 2016)	89.4	7.54	1.53	0.10	79.1	13.26	1.75	0.16
ICNet (Zhao et al., 2018)	90.8	9.48	1.84	0.05	79.4	10.81	1.43	0.13
BiSeNetV2 (Yu et al., 2021)	92.2	6.74	1.27	0.07	84.2	8.35	1.13	0.14
SegFormer (Xie et al., 2021)	90.4	10.51	1.93	0.04	80.3	11.16	1.52	0.11
U-Transformer (Petit et al., 2021)	94.1	6.81	0.84	0.06	88.4	<b>8.31</b>	1.19	0.12
SwinUNETR (Hatamizadeh et al., 2021)	94.0	5.02	1.32	0.05	88.9	10.10	1.23	0.10
SAM (2pts/slice)	68.4	16.22	3.92	0.44	-	-	-	-
SAM (1box/slice)	85.1	8.43	1.87	0.21	-	-	-	-
MediViSTA-SAM	<b>96.0</b>	<b>4.25</b>	<b>0.74</b>	<b>0.02</b>	<b>89.1</b>	8.93	<b>1.02</b>	<b>0.08</b>

In-house data	$LV_{endo}$				$LV_{epi}$				LA			
	Dice $\uparrow$	dH $\downarrow$	dA $\downarrow$	$L\downarrow$	Dice $\uparrow$	dH $\downarrow$	dA $\downarrow$	$L\downarrow$	Dice $\uparrow$	dH $\downarrow$	dA $\downarrow$	$L\downarrow$
LUNet (Leclerc et al., 2020)	87.9	14.21	6.10	0.16	75.1	15.63	7.10	0.18	84.5	18.48	4.91	0.09
Deeplabv3 (Chen et al., 2017)	88.1	13.30	5.44	0.10	74.2	13.95	6.90	0.13	85.7	16.22	4.88	0.06
Unet++ (Zhou et al., 2019)	85.1	16.34	6.42	0.19	72.2	19.43	7.49	0.21	83.5	23.04	5.91	0.07
Enet (Paszke et al., 2016)	80.4	20.12	7.02	0.16	70.6	23.23	9.92	0.24	81.2	26.21	7.11	0.12
ICNet (Zhao et al., 2018)	85.2	18.22	6.10	0.15	71.2	21.26	7.44	0.21	82.3	21.53	5.31	0.09
BiSeNetV2 (Yu et al., 2021)	86.1	16.04	4.98	0.09	73.1	20.71	5.93	0.12	84.9	19.04	5.92	0.12
SegFormer (Xie et al., 2021)	83.5	19.87	6.22	0.14	70.9	25.14	9.34	0.16	82.1	18.94	4.11	0.10
U-Transformer Petit et al. (2021)	86.2	14.52	5.11	0.18	74.2	12.34	6.85	0.18	87.1	13.22	4.02	0.08
SwinUNETR (Hatamizadeh et al., 2021)	87.8	13.98	5.88	0.18	78.4	13.29	6.73	0.16	88.9	13.11	5.22	0.19
SAM (2pts/slice)	65.2	28.46	24.18	0.74	-	-	-	-	66.2	28.11	12.24	0.45
SAM (1box/slice)	83.2	18.23	5.47	0.20	-	-	-	-	80.4	16.11	5.97	0.21
MediViSTA-SAM	<b>91.0</b>	<b>11.03</b>	<b>3.26</b>	<b>0.05</b>	<b>80.0</b>	<b>11.94</b>	<b>4.56</b>	<b>0.10</b>	<b>90.0</b>	<b>10.62</b>	<b>3.22</b>	<b>0.05</b>

data might come from diverse hospitals and vendors, each with their distinct scanning protocols. In our experiment, we evaluate the zero-shot capability of the proposed methods, which were trained on the CAMUS dataset, by testing our model on our in-house dataset. MediViSTA-SAM demonstrated a performance improvement over SwinUNETR, with a 3.18%, 1.6%, and 1.1% enhancement in the Dice coefficient and 2.62, 0.06, and 0.16 improvements in temporal smoothness for  $LV_{endo}$ ,  $LV_{epi}$ , and LA, respectively. Furthermore, we conducted an additional evaluation of the consistently high-performing MediViSTA-SAM method using critical clinical metrics. The correlation were strong showing a pearson correlation coefficient of 0.96 for LVEDV, 0.98 for LVESV, and 0.89 for EF. These high correlation scores not only validate the accuracy of our model but also highlight its trustworthiness when applied to essential clinical indicators pivotal for cardiac health evaluations. The correlation and Bland–Altman plots for these indices are presented in Figure 6.

## 6. Ablation Studies

In this section, we conduct a comprehensive examination of the various elements that make up our proposed model. We begin our assessment by evaluating the effectiveness of the spatio-temporal design and then proceed to assess the impact of integrating multi-scale fusion. We also evaluated the impact of pretrained SAM on model performance.

### 6.0.1. Spatio-Temporal Adapter Design

In this section, we investigate the impact of spatio-temporal adapter designs on the performance of our method. We conducted ablation experiments to examine the effects of cross-frame attention in our model. Our experiments demonstrate that the inclusion of cross-frame attention leads to a 0.2% improvement in Dice and a 0.03 increase in temporal smoothness, showcasing its positive impact on our method’s performance. Figure 4 provides a visual comparison of MediViSTA across frames, emphasizing the presence of ambiguous boundaries on the lateral side. Nevertheless, our model successfully captures temporal information along the time axis, resulting in segmented images with enhanced temporal smoothness. This observation highlights the inter-dependence between adjacent frames, where each frame significantly influences its neighboring frames.

To further investigate the impact of the order in which the spatio-temporal adapter is built, we conducted a comparison by reversing the order of spatial and temporal attention. The quantitative evaluation results, presented in Table 3, reveal that initiating with spatial attention, followed by temporal attention, leads to a decrease of 0.5% and an increase of 0.02, Dice and temporal consistency metric. In comparison, the concurrent application of spatial and temporal attention, as Fig 1, results in a reduction of 0.4% in the dice coefficient and a 0.02% increase in temporal smoothness. Based on these findings, we have chosen to structure the temporal and spatial attention.

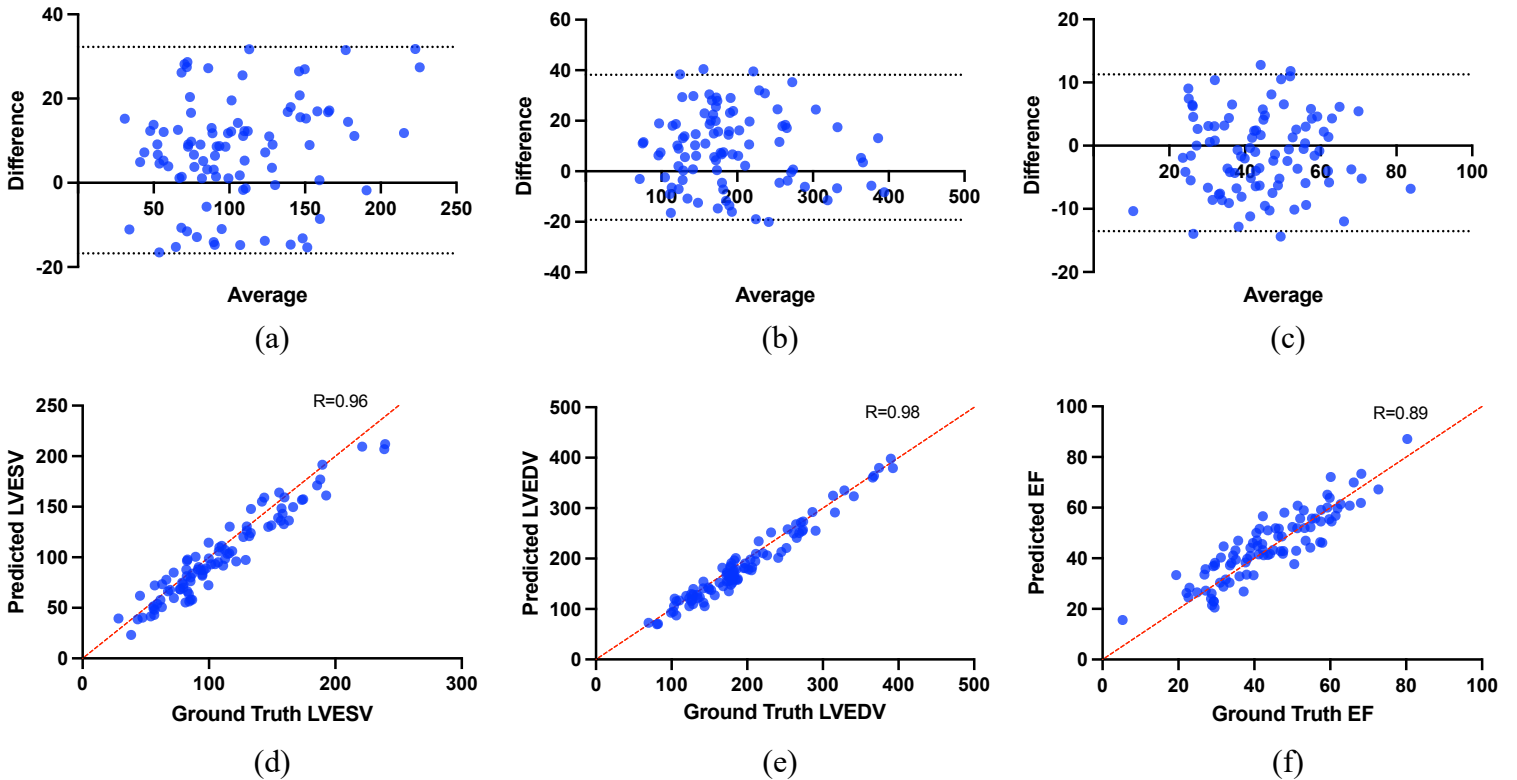


Figure 6: Comparison between automated method and manual measurement of LV volume, and ejection fraction (EF). Bland-Altman analysis and Pearson correlation plot on in-house dataset. For LVEDV, bias = 7.74; limits of agreement = -16.77 to 32.25. For LVESV, bias = 9.46; limits of agreement = -19.24 to 38.17. For EF, bias = -1.13; limits of agreement = -13.54 to 11.28. For Pearson correlation coefficient,  $r=0.96$ ,  $r=0.98$ , and  $r=0.89$ , respectively.

Table 2: An ablation study effect of cross-frame attention on model performance.

Attention	Dice [%]	L
w/o Cross-frame attention	86.8	0.09
w Cross-frame attention	87.0	0.06

### 6.0.2. Multi-scale fusion Design

To evaluate the efficacy of the multi-scale fusion approach, we conduct an ablation study focusing on the multi-scale fusion encoder and the mask decoder components. By eliminating both the multi-scale image encoder and the mask decoder, we demonstrate its effectiveness on segmentation performance. As illustrated in Table 4 (row 3 and 4), without multi-scale fusion leads to a decline in segmentation outcomes by 1.1 %, also with an increase in temporal smoothness by 0.03. Finally, we obtain the best results when both, spatio-temporal adapter and multi-scale fusion are activated.

### 6.0.3. Effectiveness of pretrained SAM

Table 5 compares the performance of the pretrained SAM using various weight types. The largest pretrained model, ViT-H, exhibits the best accuracy across all metrics, achieving the highest dice score and exhibiting low temporal smoothness. Performance decreases as the model size, resulting in the lowest dice score on ViT-b. Experiments without the pretrained SAM were conducted using the smallest model architecture comprising 12 blocks due to GPU memory constraints. Our tests showed a 4.42% decrease in dice compared to when using pretrained SAM.

Table 3: An ablation study demonstrating the impact of different spatio-temporal attention designs.

Adapter	Dice [%]	L
3D Adapter	86.6	0.09
Temporal after spatial attention	86.5	0.08
Spatial after temporal attention	87.0	0.06
Parallel attention Wu et al. (2023)	86.6	0.08

## 7. Discussion

SAM, a large-parameter vision foundation model, is a strategy for domain generalization that allows neural networks to transfer knowledge effectively to other domains, improving performance in downstream tasks. However, SAM’s performance in directly applying to medical images is unsatisfactory. This is mainly because supervised learning relies on training data distribution, which primarily consists of natural images. Additionally, 2D SAM has limitations in medical image tasks, as most modalities in clinical practice are 3D or 2DT data. Therefore, we propose MediViSTA-SAM, a method specifically designed for medical video segmentation. Our method shows improved segmentation performance in zero-shot analysis on echocardiography. We also found that the introduction of spatial attention and global and local temporal attention improves model performance for two reasons. First, it captures spatiotemporal information. We adopted a multi-scale fusion framework in our model to easily capture various object sizes. By combining these components, we achieve more robust results with fast convergence, and enhanced model generalization. Compared to other state-of-the-art methods and domain-specific approaches, our proposed method demonstrates superior performance across various metrics, including region-based, temporal, and clinical metrics.



Table 4: An ablation study on each model component’s impact on model performance.

pretrained SAM	Multi-scale fusion	Dice [%]	L
		82.1	0.14
	✓	84.8	0.11
✓		85.9	0.09
✓	✓	87.0	0.06

Table 5: An ablation study of model performance using different SAM backbones.

Backbone	Dice [%]	L
ViT-B w/o pretrained	82.1	0.17
ViT-B with pretrained	85.9	0.13
ViT-L with pretrained	86.2	0.11
ViT-H with pretrained	87.0	0.06

## 8. Conclusion

In this study, we introduce an efficient framework equipped with a parameter-efficient method for adapting the SAM model from 2D to 2DT segmentation tasks in medical videos, with a particular focus on echocardiography. To our knowledge, this is the pioneering research to investigate SAM’s capabilities for segmenting medical videos, specifically targeting echocardiography. We have developed a CNN encoder integrated with a transformer to encode input into latent space and have introduced a spatio-temporal adapter that employs both global and local temporal attention mechanisms. Through comprehensive testing, our method has shown promising results, outperforming existing state-of-the-art techniques and also in zero-shot echocardiography analysis across a multi-center dataset. This work emphasizes the growing significance of foundational model adaptation in enhancing its applicability within this domain.

## References

Bertasius, G., Wang, H., Torresani, L., 2021. Is space-time attention all you need for video understanding?, in: ICML, p. 4.

Brown, T., Mann, B., Ryder, N., Subbiah, M., Kaplan, J.D., Dhariwal, P., Neelakantan, A., Shyam, P., Sastry, G., Askell, A., et al., 2020. Language models are few-shot learners. *Advances in neural information processing systems* 33, 1877–1901.

Bui, N.T., Hoang, D.H., Tran, M.T., Le, N., 2023. Sam3d: Segment anything model in volumetric medical images. *arXiv preprint arXiv:2309.03493*.

Chen, C., Miao, J., Wu, D., Yan, Z., Kim, S., Hu, J., Zhong, A., Liu, Z., Sun, L., Li, X., et al., 2023. Ma-sam: Modality-agnostic sam adaptation for 3d medical image segmentation. *arXiv preprint arXiv:2309.08842*, 6, 9.

Chen, J., Lu, Y., Yu, Q., Luo, X., Adeli, E., Wang, Y., Lu, L., Yuille, A.L., Zhou, Y., 2021. Transunet: Transformers make strong encoders for medical image segmentation. *arXiv preprint arXiv:2102.04306*.

Chen, L.C., Papandreou, G., Schroff, F., Adam, H., 2017. Rethinking atrous convolution for semantic image segmentation. *arXiv preprint arXiv:1706.05587*.

Chen, R.J., Ding, T., Lu, M.Y., Williamson, D.F.K., Jaume, G., Song, A.H., Chen, B., Zhang, A., Shao, D., Shaban, M., et al., 2024. Towards a general-purpose foundation model for computational pathology. *Nature Medicine*, 1–13.

Defazio, A., Jelassi, S., 2022. Adaptivity without compromise: a momentumized, adaptive, dual averaged gradient method for stochastic optimization. *The Journal of Machine Learning Research* 23, 6429–6462.

Deng, G., Zou, K., Ren, K., Wang, M., Yuan, X., Ying, S., Fu, H., 2023. Sam-u: Multi-box prompts triggered uncertainty estimation for reliable sam in medical image. *arXiv preprint arXiv:2307.04973*.

Dosovitskiy, A., Beyer, L., Kolesnikov, A., Weissenborn, D., Zhai, X., Unterthiner, T., Dehghani, M., Minderer, M., Heigold, G., Gelly, S., et al., 2020. An image is worth 16x16 words: Transformers for image recognition at scale. *arXiv preprint arXiv:2010.11929*.

Fedorov, A., Beichel, R., Kalpathy-Cramer, J., Finet, J., Fillion-Robin, J.C., Pujol, S., Bauer, C., Jennings, D., Fennessy, F., Sonka, M., et al., 2012. 3d slicer as an image computing platform for the quantitative imaging network. *Magnetic resonance imaging* 30, 1323–1341.

Hatamizadeh, A., Nath, V., Tang, Y., Yang, D., Roth, H.R., Xu, D., 2021. Swin unetr: Swin transformers for semantic segmentation of brain tumors in mri images, in: *International MICCAI Brainlesion Workshop*, Springer. pp. 272–284.

Hu, E.J., Shen, Y., Wallis, P., Allen-Zhu, Z., Li, Y., Wang, S., Wang, L., Chen, W., 2021. Lora: Low-rank adaptation of large language models. *arXiv preprint arXiv:2106.09685*.

Jia, M., Tang, L., Chen, B.C., Cardie, C., Belongie, S., Hariharan, B., Lim, S.N., 2022. Visual prompt tuning, in: *Computer Vision—ECCV 2022: 17th European Conference, Tel Aviv, Israel, October 23–27, 2022, Proceedings, Part XXXIII*, Springer. p. 709–727.

Kalapos, A., Gyires-Tóth, B., 2022. Self-supervised pretraining for 2d medical image segmentation, in: *European Conference on Computer Vision*, Springer. pp. 472–484.

Khachatryan, L., Movsisyan, A., Tadevosyan, V., Henschel, R., Wang, Z., Navasardyan, S., Shi, H., 2023. Text2video-zero: Text-to-image diffusion models are zero-shot video generators, in: *Proceedings of the IEEE/CVF International Conference on Computer Vision*, pp. 15954–15964. URL: <https://example.com/text2video-zero>.

Kirillov, A., Mintun, E., Ravi, N., Mao, H., Rolland, C., Gustafson, L., Xiao, T., Whitehead, S., Berg, A.C., Lo, W.Y., et al., 2023. Segment anything. *arXiv preprint arXiv:2304.02643*.

Lang, R.M., Badano, L.P., Mor-Avi, V., Afilalo, J., Armstrong, A., Ernande, L., Flachskampf, F.A., Foster, E., Goldstein, S.A., Kuznetsova, T., et al., 2015. Recommendations for cardiac chamber quantification by echocardiography in adults: an update from the american society of echocardiography and the european association of cardiovascular imaging. *European Heart Journal-Cardiovascular Imaging* 16, 233–271.

Leclerc, S., Smistad, E., Østvik, A., Cervenansky, F., Espinosa, F., Espeland, T., Berg, E.A.R., Belhamissi, M., Israilov, S., Grenier, T., et al., 2020. Lu-net: a multistage attention network to improve the robustness of segmentation of left ventricular structures in 2-d echocardiography. *IEEE Transactions on Ultrasonics, Ferroelectrics, and Frequency Control* 67, 2519–2530.

- Mitchell, C., Rahko, P.S., Blauwet, L.A., Canaday, B., Finstuen, J.A., Foster, M.C., Horton, K., Ogunyankin, K.O., Palma, R.A., Velazquez, E.J., 2019. Guidelines for performing a comprehensive transthoracic echocardiographic examination in adults: recommendations from the american society of echocardiography. *Journal of the American Society of Echocardiography* 32, 1–64.
- openai, 2024. Sora:creating video from text. <https://openai.com/sora>.
- Painchaud, N., Duchateau, N., Bernard, O., Jodoin, P.M., 2022. Echocardiography segmentation with enforced temporal consistency. *IEEE Transactions on Medical Imaging* 41, 2867–2878.
- Pan, J., Lin, Z., Zhu, X., Shao, J., Li, H., 2022. St-adapter: Parameter-efficient image-to-video transfer learning. *Advances in Neural Information Processing Systems* 35, 26462–26477.
- Park, S., Kim, G., Oh, Y., Seo, J.B., Lee, S.M., Kim, J.H., Moon, S., Lim, J.K., Ye, J.C., 2022. Multi-task vision transformer using low-level chest x-ray feature corpus for covid-19 diagnosis and severity quantification. *Medical image analysis* 75, 102299.
- Paszke, A., Chaurasia, A., Kim, S., Culurciello, E., 2016. Enet: A deep neural network architecture for real-time semantic segmentation. *arXiv preprint arXiv:1606.02147*.
- Petit, O., Thome, N., Rambour, C., Themyr, L., Collins, T., Soler, L., 2021. U-net transformer: Self and cross attention for medical image segmentation, in: *Machine Learning in Medical Imaging: 12th International Workshop, MLMI 2021, Held in Conjunction with MICCAI 2021, Strasbourg, France, September 27, 2021, Proceedings 12*, Springer. pp. 267–276.
- Pfeuffer, A., Schulz, K., Dietmayer, K., 2019. Semantic segmentation of video sequences with convolutional lstms, in: *2019 IEEE intelligent vehicles symposium (IV)*, IEEE. pp. 1441–1447.
- Qiu, Z., Yao, T., Mei, T., 2017. Learning deep spatio-temporal dependence for semantic video segmentation. *IEEE Transactions on Multimedia* 20, 939–949.
- Radford, A., Kim, J.W., Hallacy, C., Ramesh, A., Goh, G., Agarwal, S., Sastry, G., Askell, A., Mishkin, P., Clark, J., et al., 2021. Learning transferable visual models from natural language supervision, in: *International conference on machine learning*, PMLR. pp. 8748–8763.
- Wald, T., Roy, S., Koehler, G., Disch, N., Rokuss, M., Holzschuh, J., Zimmerer, D., Maier-Hein, K., 2023. Sam. md: Zero-shot medical image segmentation capabilities of the segment anything model, in: *Medical Imaging with Deep Learning*, short paper track.
- Wang, X., Zhang, X., Cao, Y., Wang, W., Shen, C., Huang, T., 2023. Seggpt: Segmenting everything in context. *arXiv preprint arXiv:2304.03284*.
- Wu, J., Fu, R., Fang, H., Liu, Y., Wang, Z., Xu, Y., Jin, Y., Arbel, T., 2023. Medical sam adapter: Adapting segment anything model for medical image segmentation. *arXiv preprint arXiv:2304.12620*.
- Xie, E., Wang, W., Yu, Z., Anandkumar, A., Alvarez, J.M., Luo, P., 2021. Segformer: Simple and efficient design for semantic segmentation with transformers. *Advances in Neural Information Processing Systems* 34, 12077–12090.
- Yu, C., Gao, C., Wang, J., Yu, G., Shen, C., Sang, N., 2021. Bisenet v2: Bilateral network with guided aggregation for real-time semantic segmentation. *International Journal of Computer Vision* 129, 3051–3068.
- Zaken, E.B., Ravfogel, S., Goldberg, Y., 2021. Bitfit: Simple parameter-efficient fine-tuning for transformer-based masked language-models. *arXiv preprint arXiv:2106.10199*.
- Zhao, H., Qi, X., Shen, X., Shi, J., Jia, J., 2018. Icnnet for real-time semantic segmentation on high-resolution images, in: *Proceedings of the European conference on computer vision (ECCV)*, pp. 405–420.
- Zhou, Y., Chia, M.A., Wagner, S.K., Ayhan, M.S., Williamson, D.J., Struyven, R.R., Liu, T., Xu, M., Lozano, M.G., Woodward-Court, P., et al., 2023. A foundation model for generalizable disease detection from retinal images. *Nature* 622, 156–163.
- Zhou, Z., Siddiquee, M.M.R., Tajbakhsh, N., Liang, J., 2019. Unet++: Redesigning skip connections to exploit multiscale features in image segmentation. *IEEE transactions on medical imaging* 39, 1856–1867.
- Zou, X., Yang, J., Zhang, H., Li, F., Li, L., Gao, J., Lee, Y.J., 2023. Segment everything everywhere all at once. *arXiv preprint arXiv:2304.06718*.